IOP Conference Series: Earth and Environmental Science

PAPER • **OPEN ACCESS**

Stefan flow-inclusive mass transfer in a narrow cylindrical channel with a two-layer medium

IOP Conf. Series: Earth and Environmental Science **1348** (2024) 012051 doi:10.1088/1755-1315/1348/1/012051

Stefan flow-inclusive mass transfer in a narrow cylindrical channel with a two-layer medium

Volodymyr Yelisieiev[1,2], Vasyl Lutsenko[1,4], Tetiana Ruzova[3], Bahram Haddadi[3] and Michael Harasek[3]

[1]M.S. Poliakov Institute of Geotechnical Mechanics of the National Academy of Sciences of Ukraine, Simferopolska St., 2a, Dnipro, 49005, Ukraine
[2]Z.I. Nekrasov Iron & Steel Institute of the National Academy of Sciences of Ukraine, 49000, Dnipro, Academician Starodubov Sq., 1g, Ukraine
[3]TU Wien, Institute of Chemical, Environmental and Bioscience Engineering, Karlsplatz, 13, Vienna, 1040, Austria

[4]Corresponding author: VILutsenko@nas.gov.ua

Abstract. The exploration and extraction of oil, coal, and gas reserves are closely tied to mass transfer phenomena within porous and fractured rock formations. Frequently, these processes involve the adsorption or desorption, dissolution, or evaporation of certain components on the surface of the pore channels. In these cases, Stefan hydrodynamic flows arise, and although they may be individually small, they can have a noticeable impact on mass transfer and flow structure considering particular length of the channel. The authors explore the issue of inert component diffusion from the surface of a capillary into a suspension flow. The analysis involves a two-layer flow, including a central two-phase (liquid and particles) component and a near-wall flow of the fluid carrier. A certain component from the channel's surface permeates deep into the flow without interacting with the solid phase. In this research the authors solve a diffusion problem with boundary conditions that consider the presence of Stefan hydrodynamic flows. The calculations reveal that, depending on the magnitude of the Stefan flows and the length of the affected area, the porosity, and consequently, the viscosity of the two-phase flow zone can undergo significant variations.

1. Introduction

During the extraction of oil, natural gas, and coal significant emphasis is placed on the examination of the pore structure within coal and the adjacent rock formations. This fact is driven by two primary factors: the growing production volumes and the safety concerns associated with operations conducted in gas-rich areas, which entail an elevated risk of explosions.

In multicomponent systems, mass transfer typically leads to the generation of hydrodynamic flows that facilitate the transport of specific components within the flow [1]. Various hydrodynamic phenomena occur because certain components are released from the surface of a body or channel wall, whereas others are retained by this surface. These additional flows, known as Stefan flows, manifest particularly during evaporation, dissolution, adsorption, desorption, and membrane processes, where some components permeate through a membrane while others do not. Although the magnitudes of these flows and, consequently, the hydrodynamic velocities may be rather small in comparison to the primary flow, their impact can be significant due to the geometric characteristics of the channel.

Similar issues occur in porous and fractured-porous media, including materials such as rocks and coal. As mentioned in [2], the intricacies of the process at the pore scale level hold significance in these contexts. This also applies to water flow in soils, capillary processes in plants, and the circulation of blood in vessels.

In these cases, significant interest arises when the primary flow is two-phase, such as relatively concentrated suspensions. In natural settings, these can be seen in the flows of silty or clayey materials within long rock fractures. A notable example is the circulation of blood in vessels. Suspensions are often treated as non-Newtonian fluids [3-5], and for unstable suspensions, the flows are typically analyzed as having two distinct regions. In the near-wall area, the fluid is assumed to behave in a Newtonian manner, while in the central region, various models are applied, including power-law and Bingham models [4 - 8]. For instance, in recent research for describing blood flow [9 - 12], a two-layer scheme is used, where both components are considered Newtonian but with different viscosity coefficients. This simplification facilitates the analysis of mass transfer problems.

In this study, we investigate the diffusion of some passive component within a cylindrical channel where two-layer liquid moves. In this context, it is assumed that the central flow zone exhibits heterogeneity with regard to the diffusion process, meaning that certain mass transfer processes of the diffusing substance with moving inclusions may occur within this zone. It is also assumed that the diffusing component is neutral and does not interact with the heterogeneous component of the flow. Nevertheless, it should be noted that the diffusion flow generated on the vessel's walls due to the presence of this component results in additional mass transport, which, in turn, impacts the flow characteristics. Assuming that the flow within the cylindrical channel is relatively slow, i.e., it is laminar, and that the resulting distributed additional flow is negligible in comparison to the primary flow, the flow in a narrow channel can be analyzed within the framework of boundary layer theory.

Therefore, the aim of this study is to assess how Stefan flows affect the flow structure within pore channels when surface mass transfer processes are present.

2. Methods

Considered physical model is based on the well-established equation describing the laminar flow in a narrow cylindrical channel with a fixed diameter [13]

$$0 = -\frac{\mathrm{d}p}{\mathrm{d}z} + \mu_I\left(\frac{\partial^2 u_I}{\partial r^2} + \frac{\partial u_I}{r\partial r}\right), \tag{1}$$

where z – the longitudinal coordinate, m; r – radius, m; p – pressure; Pa, u – velocity, m/s; and μ – dynamic viscosity coefficient, Pa·s. The index *"I"* is used to specify the region: 1 corresponds to the near-wall region, and 2 – to the central region.

From this equation it follows that

$$u_1 = -\frac{\mathrm{d}p}{4\mu_1\mathrm{d}z}\left(1-n^2\right), \tag{2}$$

$$u_2 = -\frac{\mathrm{d}p}{4\mu_1\mathrm{d}z}\left(1-n_*{}^2 + \frac{\mu_1}{\mu_2}\left(n_*{}^2 - n^2\right)\right). \tag{3}$$

From equations (2) and (3) it follows that the average velocity is

$$U_{\mathrm{SR}} = 2\left(\int_0^{n*} n u_2\,dn + \int_{n*}^{1} n u_1\,dn\right) = -\frac{\mathrm{d}p}{4\mu_1\mathrm{d}z}\left\{1-n_*{}^2 - \frac{1}{2}\left(1-n_*{}^4\right) + \left[\left(1-n_*{}^2\right) + \frac{1}{2}\frac{\mu_1}{\mu_2}n_*{}^2\right]n_*{}^2\right\}. \tag{4}$$

Here, $n = r/Rc$, $n^* = r^*/Rc$, where Rc –capillary radius, m and r^* – radius of the two-phase zone, m.

To equation (1) should be added equation of continuity

$$\frac{\partial(\varepsilon r u_I)}{\partial z}+\frac{\partial(\varepsilon r v_I)}{\partial r}=0 \tag{5}$$

and equation describing mass transfer

$$\left(\frac{\partial \varepsilon c_I}{\partial t}+\frac{\partial \varepsilon u_I c_I}{\partial z}+\frac{\partial \varepsilon v_I c_I}{\partial r}\right)=\frac{\partial}{r\partial r}\left(rD_I\frac{\partial c_I}{\partial r}\right), \tag{6}$$

where v – transverse velocity, m/s; ε – porosity (in area 1, ε = 1); c_I – concentration of the inert component in the corresponding area; D_1 – diffusion coefficient of the component in the carrier fluid, m²/s; and D_2 – effective diffusion coefficient in region 2, m²/s. Assume that within a certain segment (z_*, z_{**}) in the primary flow, moving at a certain average velocity U_{SR}, diffuses a substance with a volumetric flow rate q_W, and no carrier liquid leaks out.

In this scenario, the following values for the flows of the diffusing substance and the solvent from the channel wall can be expressed:

$$v_W c_W - D_1\frac{\partial c_1}{\partial r}\bigg|_{r=Rc}=q_W;$$

$$v_W(1-c_W)+D_1\frac{\partial c_1}{\partial r}\bigg|_{r=Rc}=0. \tag{7}$$

Summing up these expressions, it is obtained that $v_W = q_W$, indicating that the diffusing flow of the considered component in a binary mixture causes mass velocity on the surface equal to the flow magnitude.

When specifying the concentration c_W of the diffusing component at the wall, the mass flow velocity is evaluated iteratively using the formula $v_W=-\frac{D_1}{(1-c_W)}\frac{\partial c_1}{\partial r}\Big|_{r=Rc}$. Furthermore, assume that the transverse flow is negligible and does not disrupt the flow structure. Therefore, porosity is dependent solely on the longitudinal coordinate. Substituting the longitudinal velocities from equations (2) and (3) into the continuity equation, the following expressions for transverse velocities may be obtained:

$$v_1=\frac{A}{n}-\frac{1}{16}Rc\frac{\mathrm{d}B}{\mathrm{d}z}\left(2n-n^3\right),\quad A=v_W+\frac{1}{16}Rc\frac{\mathrm{d}B}{\mathrm{d}z}; \tag{8}$$

$$v_2=-\frac{1}{16}Rc\frac{\mathrm{d}\varepsilon B}{\varepsilon\mathrm{d}z}\left\{2\left[1-\left(1-\frac{\mu_1}{\mu_2}\right)n_*^{\,2}\right]n-\frac{\mu_1}{\mu_2}n^3\right\},\quad B=\frac{Rc^2}{\mu_1}\frac{\mathrm{d}p}{\mathrm{d}z}. \tag{9}$$

In this scenario, it's essential to consider that at the regions' boundaries $r = r_*$ $v_1 = \varepsilon v_2$.

If equations (8) and (9) are inserted into this condition and then multiplied by 2π, the mass conservation condition may be derived, allowing the pressure to be evaluated:

$$2\pi Rc\left\{\frac{B}{16}\left[1-n_*\left(2n_*-n_*^{\,3}\right)\right]+\frac{\varepsilon B}{16}\left\{2\left[1-\left(1-\frac{\mu_1}{\mu_2}\right)n_*^{\,2}\right]n_*^{\,2}-\frac{\mu_1}{\mu_2}n_*^{\,4}\right\}\right\}=2\pi Rc\int_{z^*}^{Z}Vw\mathrm{d}z+Q_G, \tag{10}$$

where $B = (Rc)^2(\mathrm{d}p/\mathrm{d}z)$, and Q_G is the initial flow of the carrier fluid.

The condition of mass conservation for the heterogeneous component is then introduced.

$$2\pi Rc\frac{(1-\varepsilon)B}{16}\left\{2\left[1-\left(1-\frac{\mu_1}{\mu_2}\right)n_*^{\,2}\right]n_*^{\,2}-\frac{\mu_1}{\mu_2}n_*^{\,4}\right\}=Q_C, \tag{11}$$

where Q_C is the consumption of the dispersed phase.

The presented equations are completed with symmetry conditions along the tube axis and with the dependences between the effective diffusion D_2 and effective viscosity with porosity ε. Following [14], diffusion coefficient in the central region may be expressed as follows:

$$D_2 = f(\varepsilon)D_1, \quad f(\varepsilon) = \varepsilon\left[1 - \frac{2}{3}(1+\varepsilon)(1-\varepsilon)^{3/2}\right]. \tag{12}$$

To calculate effective viscosity, the following equation [15] is applied:

$$\mu_2 = \left(1 + 0.75\frac{\tau(\tau_P)^{-1}}{1-\tau(\tau_P)^{-1}}\right)^2 \mu_1, \tag{13}$$

where, $\tau = (1 - \varepsilon)$, $\tau_P = 0.7$ represents the maximum filling value.

Then two scenarios are investigated: in the first one, the flow rate q_W of the diffusing component in a some channel segment (z_*, z_{**}) is pre-specified, and in the second case, the concentration c_W within the same segment is pre-specified.

3. Results and discussion

The problem was numerically solved using a finite-difference scheme, which is commonly employed in mass transfer calculations, as demonstrated in [16, 17], for instance. The results of calculations for the scenario with pre-specified diffusing substance flow are shown in figures 1 – 4. The calculations were conducted with the following parameters: tube length $L = 0.1$ m; radius $Rc = 5\cdot10^{-4}$ m; $z_* = 0.01$m; $z_{**} = 0.09$ m; $r_* = 0.98$Rc; $D_1 = 1\cdot10^{-9}$ m²/s; initial average velocity $U_{SR0} = 0.002$ m/s.

The initial porosity ε_0 was set to values of 0.5, 0.6, 0.7, and 0.8.

Figure 1 illustrates the porosity profiles along the channel axis for two cases, when $q_W = -0.005U_{SR0}$ (thick lines) and for $q_W = 0.01U_{SR0}$ (thin lines). These curves show that, even with a low flow rate q_W of the component introduced into the channel, the two-phase zone expands due to the length of the input segment. This expansion is associated with the velocity increase due to additional increments in the total flow magnitude.

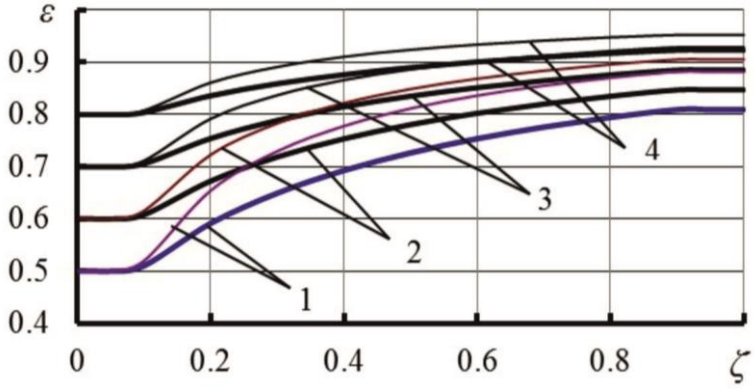

Figure 1. Porosity profiles along the channel axis $\zeta = z/L$.

$1 - \varepsilon_0 = 0.5$; $2 - \varepsilon_0 = 0.6$; $3 - \varepsilon_0 = 0.7$; $4 - \varepsilon_0 = 0.8$.

Figure 2 shows the concentration increase along the flow c_S axis for two scenarios: one with $q_W = -0.005\cdot U_{SR0}$ (thick lines) and the other with $q_W = -0.01\cdot U_{SR0}$ (thin lines). It's evident that the curves are monotonic, and, as expected, higher values of q_W lead to faster saturation with the injected component.

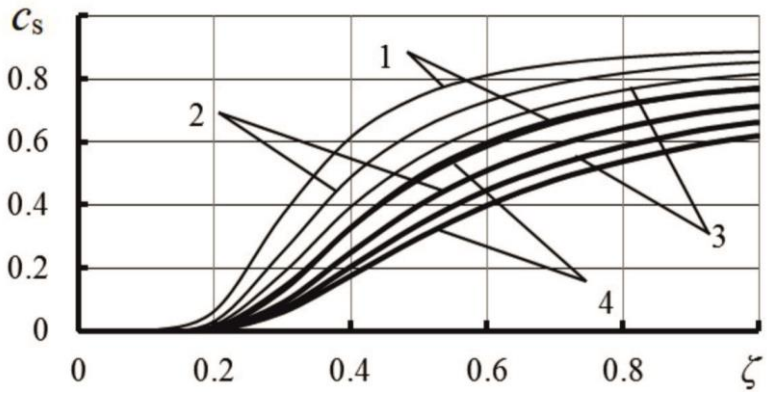

Figure 2. Concentration profiles c_S of the diffusing substance along the channel axes $\zeta = z/L$.
1 – ε = 0.5; 2 – ε = 0.6; 3 – ε = 0.7; 4 – ε = 0.8.

Figure 3 presents the concentration curves c_L at the cross-section of the channel outlet, at $\zeta = 1$. The provided concentration profiles reveal that in the central region of the channel, the concentration values are slightly lower than those at the wall. This is expected since the substance was introduced from the wall. Furthermore, the curves exhibit a noticeable maximum slightly away from the wall. This phenomenon is a result of the fact that the length of the segment through which the component was introduced is slightly shorter than the overall channel length, and the remaining zone is filled with the diffusing substance from adjacent levels.

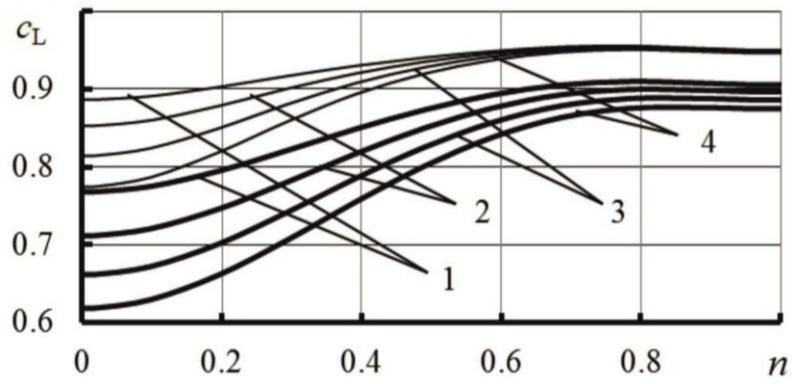

Figure 3. Alterations in the concentrations (c_L) of the diffusing substance in the outlet section across the channel radius $n = r/Rc$ (1 – ε_0 = 0.5; 2 – ε_0 = 0.6; 3 – ε_0 = 0.7; 4 – ε_0 = 0.8).

The next figure 4 clearly depicts the alteration in the overall flow velocity resulting from the introduction of additional mass. In this case, the lower set of curves (dashed lines) represents the initial velocity profile in the channel. The middle group (thick lines) corresponds to $q_{W=}$ - $0.005 \cdot U_{SR0}$, and the upper group (thin lines) corresponds to $q_{W=}$ - $0.01 \cdot U_{SR0}$. From the figure it is evident that altering the initial porosity from 0.5 to 0.8 has almost no impact on the longitudinal velocity profiles at the end of the channel. At the scale of this figure, all curves 1 – 4 appear to merge into a single line. It is also evident that due to the influence of the segment length (z_*, z_{**}), different diffusion flow magnitudes result in significant variations in the total flow rate at the channel outlet, leading to significant alterations in the velocity profiles at the end of the channel.

The following figures 5–8 display the same curves for the second calculations set, where

concentration values were specified within the same segment of the wall (z_*, z_{**}). In this series two cases were investigated: $c_W = 0.4$ and $c_W = 0.8$, with $U_{SR0} = 0.001$.

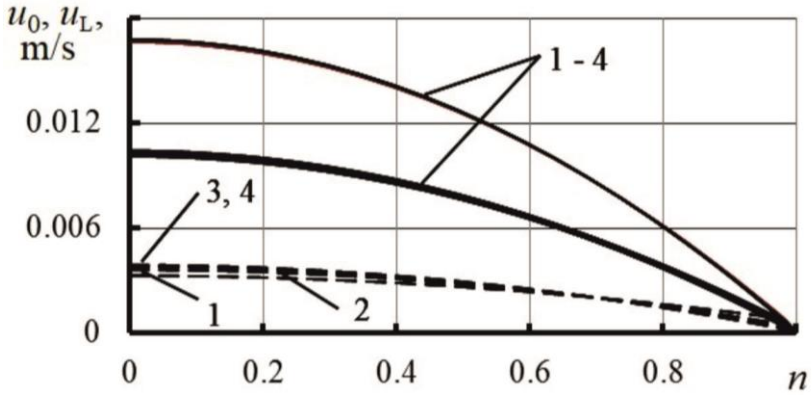

Figure 4. Longitudinal velocity profiles at the channel inlet (u_0, dashed lines) and outlet (u_L, solid lines) ($1 - \varepsilon_0 = 0.5$; $2 - \varepsilon_0 = 0.6$; $3 - \varepsilon_0 = 0.7$; $4 - \varepsilon_0 = 0.8$).

Figure 5 demonstrates that specifying the concentration on the wall also gives rise to an additional flow into the channel (its magnitude is calculated using the formula $q_W = -\frac{D_1}{(1-c_W)}\frac{\partial c_1}{\partial r}\Big|_{r=Rc}$), which, in turn, leads to an expansion of the two-phase zone (thick lines correspond to $c_W = 0.4$, while thin lines represent $c_W = 0.8$).

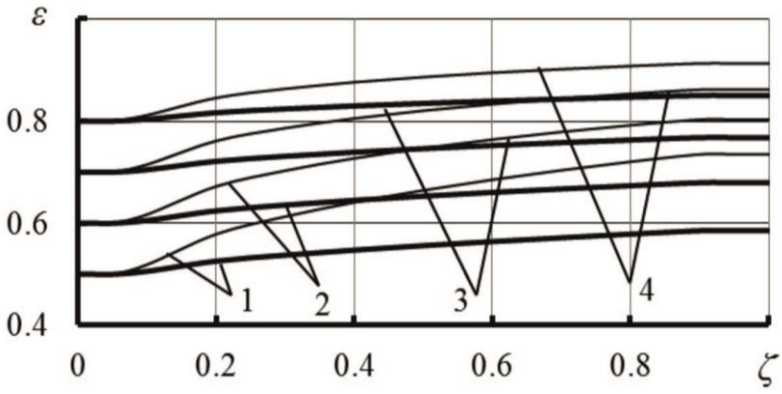

Figure 5. Porosity profiles along the channel axis $\zeta = z/L$. $1 - \varepsilon_0 = 0.5$; $2 - \varepsilon_0 = 0.6$; $3 - \varepsilon_0 = 0.7$; $4 - \varepsilon_0 = 0.8$.

Figure 6 illustrates the increase in concentrations along the channel axis. The curves appear to be divided into two groups based on the specified concentration values, and within each group, the curves exhibit slight differences from one another. A similar pattern is observed in figure 7, which presents the concentration profiles at the channel outlet. In this figure as well, there are two groups of curves, within each group curves positioned quite closely to each other.

The last figure 8 presents the longitudinal velocity profiles at the channel inlet and outlet. Dashed lines correspond to the initial profile, thick lines – to the final profile for $c_W = 0.4$, and thin lines correspond to $c_W = 0.8$, respectively. When comparing this figure with figure 4, it becomes evident that the impact of the additional flow here is diminished, but still notably visible, particularly for $c_W = 0.8$.

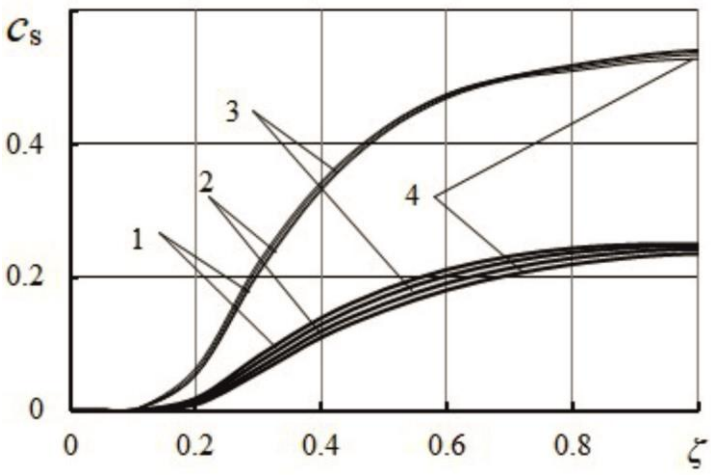

Figure 6. Concentration profiles c_S of the diffusing substance along the channel axes $\zeta = z/L$ (1 – ε_0 = 0.5; 2 – ε_0 = 0.6; 3 – ε_0 = 0.7; 4 – ε_0 = 0.8, lower curves group corresponds to c_W = 0.4, upper group – to c_W = 0.8).

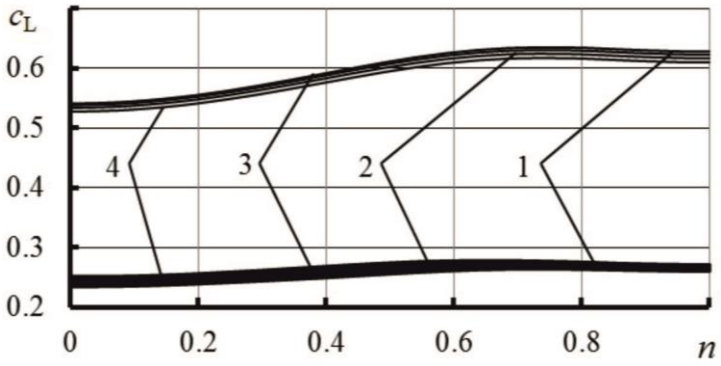

Figure 7. Alterations in the concentrations c_L of the diffusing substance in the outlet section across the channel radius $n = r/Rc$ (1 – ε_0 = 0.5; 2 – ε_0 = 0.6; 3 – ε_0 = 0.7; 4 – ε_0 = 0.8, lower curves group corresponds to c_W = 0.4, upper group – to c_W = 0.8).

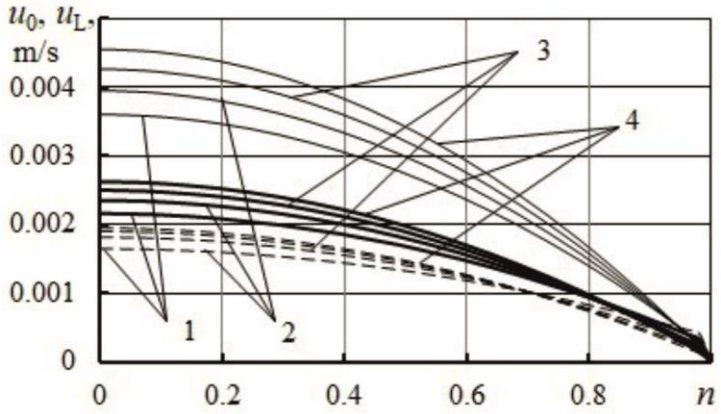

Figure 8. Longitudinal velocity profiles at the channel inlet (u_0) and outlet (u_L) (1 – ε_0 = 0.5; 2 – ε_0 = 0.6; 3 – ε_0 = 0.7; 4 – ε_0 = 0.8).

4. Conclusions

In this research the authors explores scenarios in which the introduction of an additional component into the flow leads to the formation of supplementary mass flows. While the magnitudes of these flows are relatively small compared to the primary flow, their cumulative effect, considering the length of the supply zone, can be comparable to that of the primary flow, significantly affecting the characteristics of the overall flow. The calculations demonstrated that the porosity and, consequently, the viscosity of the two-phase flow zone can vary significantly, depending on the magnitude of the Stefan flows and the length of the impact zone.

The results of this research could have practical relevance when analyzing flows in fractured and

stratified rocks, especially in the context of considering the dissolution of surface layers or the presence of gas adsorption/desorption. This research has potential applications in various fields, including the development of coal seams, oil and gas production, the development of new technologies for geological CO_2 storage, and the engineering design of geotechnical structures. It can also be useful for studying the transport of pollutants in rocks and soils.

References

[1] Frank-Kamenetskii D A 1987 *Diffusion and heat transfer in chemical kinetic*s (Nauka: Moscow) p 502
[2] Guanxi Yan, Zi Li, Sergio Andres Galindo Torres, Alexander Scheuermann and Ling Li 2022 Transient Two-Phase Flow in Porous Media *A Literature Review and Engineering Application in Geotechnics Geotechnics* **2** pp. 32-90 https://doi.org/10.3390/geotechnics2010003
[3] Kulagin V and Baranova M 2011 *Physico-chemical basis for the production of coal-water suspensions* (Krasnoyarsk: SFU Publ.) p 160
[4] Pankov A O 2007 *Calculation of hydrotransport processes for non-structural suspensions in both heterogeneous and homogeneous flow modes*. Thesis for academic degree of Candidate of Technical Sciences: 05.17.08. Kazan. KSTU 126s. RGBOD. 61:07-5/2631
[5] Transport of unstable, highly concentrated suspensions in underground cavities *Mining information and analytical bulletin* pp 343-346. Available from: https://www.giab-online.ru/files/Data/2008/1/37_SHubin18.pdf
[6] Ku David N 1997 Blood flow in arteries *Annual Rev. Fluid Mech.* **29** pp 399-434
[7] Annord Mwapinga, Eunice Mureithi, James Makungu and Verdiana Masanja 2020 Non-Newtonian heat and Mass transfer on MHD blood flow through a stenosed artery in the presence of body exercise. And chemical reaction *Commun. Math. Biol. Neurosci*. **2020** 64 pp 1-27 https://doi.org/10.28919/cmbn/4906
[8] Shabrykina N S 2005 Mathematical modeling of microcirculatory processes *Russian Journal of Biomechanics* 9 (3) pp 70-88
[9] Van de Vosse F N and van Dongen M E H 1998 *Cardiovascular Fluid Mechanics* – lecture notes (Eindhoven University of Technology) p 122
[10] Manisha Vinay, Nasha Surendra and Kumar 2021 MHD Two-Layered Blood Flow Under Effect of Heat and Mass Transfer in Stenosed Artery with Porous Medium *Int. J. of Advanced Research in Eng. and Tech. (IJARET)* **12** (6) pp 63-76 DOI: 10.34218/IJARET.12.6.2021.007 Article ID: IJARET_12_06_007.pdf
[11] Chakravarty S and Sen S 2005 Dynamic response of heat and mass transfer in blood flow through stenosed bifurcated arteries *Korea-Australia Rheology Journal* **17** (2) pp 47-62 Article ID: KR17-2-0047.pdf
[12] Bhavya Tripathi, Bhupendra Kumar Sharma and Madhu Sharma 2018 MHD Pulsatile Two-Phase Blood Flow Through a Stenosed Artery with Heat and Mass Transfer *Physics Fluid Dynamics* pp 1-24 ArXiv: 1705.09794.pdf https://doi.org/10.48550/arXiv.1705.09794
[13] Lojtsansky L G 2003 *Mechanics of a Liquid and Gas*, 7th Edition (Drofa: Moscow)
[14] Kheifets L I and Neimark A V 1982 *Multiphase processes in porous media* (Moscow: Khimiya Publ.) p 320
[15] Moshev V V and Ivanov V A 1990 *Rheological Behavior of Concentrated Non-Newtonian Suspensions* (Moscow: Nauka) p 88
[16] Belyaev N N and Kirichenko P S 2017 Evaluation of air pollution levels near the dump using computational experiments. *Bulletin of Dnipropetrovsk University. Series Mechanics* **21** pp 44-5
[17] Bulat A F, Yeliseyev V I, Sovit Yu P, Molchanov R N and Blyuss O B 2019 Mathematical modeling of convective-diffusion mass transfer within a hemodialysis machine cell *Reports of the National Academy of Sciences of Ukraine*, No. 02 pp. 40-44.